A simplified multiscale damage model for the transversely isotropic shale rocks under tensile loading

Mohaddeseh Mousavi Nezhad[1], Hehua Zhu[2], J. Woody Ju[3] and Qing Chen[4,2,1*]

Abstract

A simplified multiscale damage model is proposed for the transversely isotropic shale rocks under tensile loading. In this framework, the multiscale representations for the shale rocks are presented by introducing the microcrack-weakened equivalent solid with hierarchical microstructures, whose transversely isotropic properties are obtained by performing multilevel homogenization procedures. To simplify the calculation process for the damage induced properties, the equivalent isotropic medium is attained by applying the Voigt–Reuss–Hill averaging process to the transversely isotropic solid. Subsequently, the microcrack-induced inelastic compliances are approximately derived in terms of microcrack opening displacements in the equivalent isotropic medium of the shale rock under tensile loading. The sizes and orientations of microcracks are taken as random variables. Both stationary and evolutionary damage models are considered. Microcrack kinetic equations are characterized through the use of a fracture mechanics-based stability criterion and microcrack geometry within a representative volume element. Numerical examples including experimental validations and comparisons with existing micromechanical models are presented to verify the proposed multiscale damage model. Finally, the influences of the silt inclusions and porosity on the material intrinsic and damage-induced properties are discussed.

Keywords
Multiscale damage mechanics, multilevel homogenization, transversely isotropic medium, micromechanics, shale rocks, tensile loading.

[1] Computational Mechanics, Civil Research Group, School of Engineering, University of Warwick, Warwick CV47AL, UK

[2] Key Laboratory of Geotechnical and Underground Engineering of the Ministry of Education, Tongji University, 1239 Siping Road, Shanghai 200092, China

[3] Department of Civil and Environmental Engineering, University of California, Los Angeles, CA 90095, USA

[4] Key Laboratory of Advanced Civil Engineering Materials (Tongji University), Ministry of Education, 1239 Siping Road, Shanghai 200092, China

*Corresponding author:

Qing Chen, Key Laboratory of Advanced Civil Engineering Materials (Tongji University), Ministry of Education, 1239 Siping Road, Shanghai 200092, China

E-mail: 13585546170@163.com

Introduction

Featuring hierarchical microstructures, shale rocks are anisotropic and heterogeneous, and are particularly critical for success of many fields of petroleum engineering. Shale rocks may also be important for the development of sustainable nuclear waste storage solutions (Thomsen, 2001; Ulm and Abousleiman, 2006).

Owing to these direct economic impacts of shale rocks, many efforts have been dedicated to modeling the material mechanical performance (cf. Hornby et al., 1994; Sayers, 1994, 1999, 2005; Johnston and Christensen, 1995; Levin and Markov, 2005; Chang et al., 2006; Giraud et al., 2007; Ortega et al., 2007; Farrokhrouz et al., 2014; Dewhurst et al., 2015). In general, the current research on modeling the mechanical behavior of shale rocks can be classified into two categories. The first category focuses on the empirical formulations to evaluate the properties of shale rocks by means of laboratory or site tests, which belong to the phenomenological methodology (Chang et al., 2006; Farrokhrouz et al., 2014; Dewhurst et al., 2015). The main limitation of such traditional approach is that it requires extensive and costly experimental programs to characterize the material properties. An attractive alternative is provided by the framework of micromechanics, which reduces the laboratory expenses and helps us throwing light upon the relations between the complicated material microstructures and macroscopic properties of shale rocks (Hornby et al., 1994; Levin and Markov, 2005; Giraud et al., 2007; Ortega et al., 2007).

Despite many attempts, micromechanical or multiscale damage models based on shale rocks' complex microstructures are limited compared with damage models at the macroscopic level using continuum damage mechanics (cf. Krajcinovic, 1984; Simo and Ju, 1987a, b, 1989;

Ju, 1989; Ju et al., 1989). Sayers and Kachanov (1995) and Sayers (2005) introduced micromechanical models to link elastic wave velocity data and damage of shale rocks. Their micromechanical models are effective for the case of an isotropic matrix. Ougier-Simonin et al. (2009) presented a new micromechanical damage model to extend the original method of Sayers and Kachanov (1995) to a transversely isotropic matrix containing cracks. On one hand, similar to the existing micromechanical damage models for brittle solids by Sumarac and Krajcinovic (1987), Fanella and Krajcinovic (1988), Krajcinovic and Sumarac (1989), Ju (1991) and Ju and Lee (1991), existing micromechanical damage models for shale rocks (cf. Sayers and Kachanov, 1995; Sayers, 2005; Ougier-Simonin et al., 2009) describe the material as a *two-phase* composite, including the homogeneous matrix phase and the microcrack phase. This treatise means that the porosity, clay particles, quartz inclusions and the other components of shale rocks are not taken into considerations, even though they play important roles in determining the material mechanical behaviours. On the other hand, existing micromechanical damage models for shale rocks (cf. Sayers and Kachanov, 1995; Sayers, 2005; Ougier-Simonin et al., 2009) ignored the propagations of pre-existing microcracks, which implied that the evolutionary microcrack-induced damage were not considered (cf. Budiansky and O'Connell, 1976; Hoenig, 1979; Horii and Nemat-Nasser, 1983, 1985; Chudnovsky et al., 1987a, b; Kachanov, 1987).

As an extension of existing micromechanical damage models for shale rocks, a simplified multiscale damage model for shale rocks under tensile loading is presented in this paper. In our proposed framework, the material complex microstructures, such as the clay particles, the porosity and quartz inclusions, are comprehensively considered by a multilevel homogenization scheme. Meanwhile, the microcrack propagations are considered by introducing a fracture

mechanics-based stability criterion. Further, inspired by Ougier-Simonin et al (2009), the Voigt–Reuss–Hill averages of the transversely isotropic medium are utilized to attain an equivalent isotropic matrix to simplify the calculation process.

The remainder of this paper is organized as follows. The basis of the multiscale damage model for microcracked shale rocks is first introduced in Section 2. Section 3 presents a multiscale model for microcracked shale rocks based on the material microstructures. In Section 4, the undamaged elastic compliance tensor of shale rock is obtained by the multilevel homogenization procedures. Section 5 renders the damage-induced compliance tensors of shale rocks with the microcrack opening displacements in the equivalent isotropic medium. Numerical examples including experimental validations and comparisons with existing micromechanical models are presented in Section 6, featuring detailed discussions on the influences of quartz inclusions and porosity upon the damage evolutions of shale rocks, emanating from our proposed multiscale damage framework. Significant conclusions are reached in the final section.

Basis of multiscale damage model for microcracked shale rocks

We follow Ju and Lee (1991) to summarize the basis of the multiscale damage model for shale rock There is a one-to-one correspondence between the fourth-order elastic damage compliance tensor $\mathbf{S}$ and the fourth-order anisotropic damage tensor $\mathbf{D}$. Therefore, the secant compliance $\mathbf{S}$ can be viewed as an anisotropic damage tensor. Within the framework of the homogenization concept for an inhomogeneous effective continuum medium, the volume-average strain tensor $\overline{\mathbf{\varepsilon}}$ can be expressed by the following expression

$$\overline{\mathbf{\varepsilon}} = \overline{\mathbf{S}} : \overline{\mathbf{\sigma}} \tag{1}$$

4

where $\bar{\boldsymbol{\sigma}}$ is the volume-average stress tensor and $\bar{\mathbf{S}}$ is the volume average compliance tensor.

Furthermore, it is assumed that the strain tensor $\bar{\boldsymbol{\varepsilon}}$ and the overall compliance tensor $\bar{\mathbf{S}}$ are amenable to an additive decomposition:

$$\bar{\boldsymbol{\varepsilon}} = \bar{\boldsymbol{\varepsilon}}^{e} + \bar{\boldsymbol{\varepsilon}}^{*}; \qquad \bar{\mathbf{S}} = \bar{\mathbf{S}}^{0} + \bar{\mathbf{S}}^{*} \tag{2}$$

where $\bar{\boldsymbol{\varepsilon}}^{e}$ and $\bar{\boldsymbol{\varepsilon}}^{*}$ = the elastic and the damage-induced strains, respectively. Similarly, $\bar{\mathbf{S}}^{0}$ and $\bar{\mathbf{S}}^{*}$ = the undamaged elastic and the damage-induced compliance, respectively. Implicitly, it has been assumed that $\bar{\boldsymbol{\varepsilon}}^{*} << 0$ upon complete unloading; i.e., the residual strain at zero stress is negligible.

To characterize the mechanical performance of shale rock under tensile loading in this paper, the undamaged elastic tensor of shale rock is obtained by a multi-scale approach using the transversely isotropic properties of clay particles at nanoscale level. Meanwhile, the damage-induced compliance tensor is reached by utilizing the microcrack opening displacement in the equivalent isotropic matrix for the transversely isotropic porous shale rock.

Multiscale model of microcracked shale rocks

The microstructures of shale rocks

Shale rocks are heterogeneous in nature and they generally consist of different constituents or phases, such as the clay material, quartz and calcite. Further, the constituents of materials can be treated as homogeneous at a certain length scale, but when observed at a smaller length scale, the constituents themselves may become heterogeneous; i.e., the multiscale phenomenon for heterogeneous shale rock materials (cf. Bayuk et al., 2008; Bobko and Ulm, 2008; Bobko et al., 2011; Guo et al., 2013;). For examples, according to Guo et al. (2013), the components of shale

rocks should contain clays, kerogen, cracks, pores, quartz, calcite and dolomite. The material properties are dependent on the microstructural parameters such as the orientation of clay platelets and cracks, pore/crack connectivity and shale mineralogical composition, including quartz, calcite and dolomite (Bayuk et al., 2008). The clay mineralogy should be made up of kaolinite, illite, smectite and chlorite, etc. (Bobko and Ulm, 2008). There were considerable other research work to characterize the shale rock microstructures and properties at different length scales; e.g., Chen et al. (2014a), Josh et al. (2012) and Chen et al. (2014b).

The RVE representations for microcracked shale rocks

To characterize the heterogeneous and multiscale characters of microcrack weakened shale rocks, the following procedures are performed to define the representative volume element (RVE).

Firstly, the RVE for the cracked porous shale rock is composed of a solid matrix, micropores and microcracks. The two types of defects (micropores and microcracks) can be treated by the decomposition procedures as Fig. 1(a) shows (cf. Xie et al., 2012; Yan et al., 2013; Zhu et al., 2014). The ensemble of the solid phase and pores therein is taken as a homogenized porous matrix, since the focus here is on the characterization of inelastic behaviours induced by microcracking, the effects of which are much more dominant than those of micropores (Ju and Lee, 1991; Xie et al., 2012). It is noted that the microcracks are assumed to be coin-shaped and the pores are spherical (Yan et al., 2013; Zhu et al., 2014). Furthermore, as displayed in Fig. 1(b), multiscale representations for the solid phase of shale rock is proposed to quantitatively investigate the effects of other components, such as the clay particles, quartz and calcite

6

inclusions, on the damage evolutions based on material microstructures (Bayuk et al., 2008; Bobko and Ulm, 2008; Bobko et al., 2011; Guo et al., 2013). In the multiscale representations, the inclusions (e.g., quartz, dolomite and calcite) are assumed to be spherical and well bonded with the clay matrix.

The undamaged elastic compliance tensor of shale rock

Multilevel micromechanical homogenizations for the properties of the solid matrix

For a multiphase composite, the multilevel homogenization process is usually employed to quantitatively estimate the composite effective properties (Ju and Chen, 1994a, b; Ju and Zhang, 1998; Li et al., 1999; Ju and Sun, 1999, 2001; Ju and Yanase, 2010, 2011; Chen et al., 2015a, b, c; Zhu et al., 2015).

The solid matrix of shale rock can be regarded as a multiphase composite with the clay particles as the matrix phase and the other components (e.g., quartz, calcite and dolomite) as the multi-inclusions. Based on the multilevel homogenization scheme, the equivalent matrix composed of clay particles and quartz can be obtained after the first-level homogenization, which can be expressed as follows according to Berryman (1980) and Norris (1985):

$$c_q\left(\left(\mathbf{C}_q-\mathbf{C}_{e1}\right)^{-1}+\mathbf{P}^q\right)^{-1}+c_c\left(\left(\mathbf{C}_c-\mathbf{C}_{e1}\right)^{-1}+\mathbf{P}^c\right)^{-1}=0 \tag{3}$$

with

$$c_q=\frac{V_q}{V_q+V_c} \qquad c_c=\frac{V_c}{V_q+V_c} \tag{4}$$

where c_q and c_c (V_q and V_c) are, respectively, the volume fraction (volume) of the quartz

and clay particles; $\mathbf{P}^q$ and $\mathbf{P}^p$ are the Hill polarization tensor of the quartz and porous composite, respectively; $\mathbf{C}_{e1}$ is the effective stiffness tensor of the equivalent matrix after the first level homogenization.

When the calcite inclusion is added, the effective properties of the composite made up of the clay particles, the quartz and the calcite can be expressed as

$$c_{ca}\left(\left(\mathbf{C}_{ca}-\mathbf{C}_{e2}\right)^{-1}+\mathbf{P}^{ca}\right)^{-1}+c_{e1}\left(\left(\mathbf{C}_{e1}-\mathbf{C}_{e2}\right)^{-1}+\mathbf{P}^{e1}\right)^{-1}=0 \tag{5}$$

with

$$c_{ca}=\frac{V_{ca}}{V_q+V_c+V_{ca}} \qquad c_{e1}=\frac{V_q+V_c}{V_q+V_c+V_{ca}} \tag{6}$$

where c_{ca} and c_{e1} are, respectively, the volume fraction of the calcite inclusion and the equivalent matrix obtained by the first level homogenization; V_{ca} is the volume of the calcite inclusion; $\mathbf{P}^{ca}$ and $\mathbf{P}^{e1}$ are the Hill polarization tensor of the calcite and the equivalent matrix, respectively. Moreover, $\mathbf{C}_{e2}$ is the effective stiffness tensor of the equivalent matrix obtained by the second level homogenization.

As to the other types of inclusions, the multilevel homogenization scheme can be similarly applied to obtain the effective properties of the solid matrix of shale rocks.

Micromechanical homogenization for properties of the pores-weakened solid matrix

Let $\mathbf{C}_{sm}$ represent the effective stiffness tensor of the solid matrix of shale rock. On the basis of Berryman (1980) and Norris (1985), the effective properties of the porous shale rock matrix can be written as:

8

$$c_{po}\left(\left(\mathbf{C}_{po} - \mathbf{C}_{pm}\right)^{-1} + \mathbf{P}^{po}\right)^{-1} + c_{sm}\left(\left(\mathbf{C}_{sm} - \mathbf{C}_{pm}\right)^{-1} + \mathbf{P}^{sm}\right)^{-1} = 0 \tag{7}$$

with

$$c_{po} = \frac{V_{po}}{V_{sm} + V_{po}} \qquad\qquad c_{sm} = \frac{V_{sm}}{V_{sm} + V_{po}} \tag{8}$$

where c_{po} and c_{sm} (V_{po} and V_{sm}) are the volume fraction (volume) of the micropores and solid matrix of shale rock, respectively; $\mathbf{P}^{po}$ and $\mathbf{P}^{sm}$ are the Hill polarization tensor of the pores and solid matrix of shale rock, respectively; $\mathbf{C}_{pm}$ is the effective stiffness tensor of the pores-weakened solid matrix, with which the undamaged elastic compliance tensor of shale rock can be expressed as

$$\bar{\mathbf{S}}_0 = \left(\mathbf{C}_{pm}\right)^{-1} \tag{9}$$

The damage-induced compliance tensor of shale rock under tensile loading

The equivalent isotropic medium for the pores-weakened solid matrix of shale rock

It is complex to obtain the crack-induced compliance tensor in a porous shale rock matrix, which is transversely isotropic (Sarout and Guéguen, 2008a, 2008b). Instead of performing the difficult calculation directly, a simplified approach is employed by introducing the equivalent isotropic matrix for the transversely isotropic one inspired by the work of Ougier-Simonin et al. (2009). The properties of the equivalent isotropic matrix can be characterized using the Voigt–Reuss–Hill average of the properties of the transversely isotropic pores-weakened solid matrix by the following expressions (Ulm and Abousleiman, 2006; Ougier-Simonin et al., 2009):

9

$$K_{VRH} = \frac{1}{2}\left(K_V^{pm} + K_R^{pm}\right); \quad G_{VRH} = \frac{1}{2}\left(G_V^{pm} + G_R^{pm}\right) \tag{10}$$

with

$$K_V^{pm} = \frac{1}{9}\left(2C_{11}^{pm} + C_{33}^{pm}\right) + \frac{2}{9}\left(C_{12}^{pm} + 2C_{13}^{pm}\right) \tag{11}$$

$$G_V^{pm} = \frac{1}{15}\left(2C_{11}^{pm} + C_{33}^{pm}\right) - \frac{1}{15}\left(C_{12}^{pm} + 2C_{13}^{pm}\right) + \frac{1}{5}\left(2C_{44}^{pm} + C_{66}^{pm}\right) \tag{12}$$

$$K_R^{pm} = \frac{1}{A(C_{11}^{pm} + C_{12}^{pm} + 2C_{33}^{pm} - 4C_{13}^{pm})} \tag{13}$$

$$G_R^{pm} = \frac{15}{2A\left(2\left(C_{11}^{pm} + C_{12}^{pm}\right) + 4C_{13}^{pm} + C_{33}^{pm}\right) + \frac{1}{6}\left(1/C_{44}^{pm} + 1/C_{66}^{pm}\right)} \tag{14}$$

$$A = \frac{1}{C_{33}^{pm}\left(C_{11}^{pm} + C_{12}^{pm}\right) - 2\left(C_{13}^{pm}\right)^2} \tag{15}$$

where $C_{ij}^{pm}\left(i, j = 1, 2, 3, 4, 5, 6\right)$ are the components of the stiffness tensor of the pores-weakened solid matrix; K_{VRH} and G_{VRH} are the bulk modulus and shear modulus of the equivalent isotropic matrix, respectively. According to the relationships between the elastic constants of the isotropic materials, the Young's modulus and Poisson's ratio can be obtained as follows:

$$E_{VRH} = \frac{9K_{VRH}G_{VRH}}{3K_{VRH} + G_{VRH}} \tag{16}$$

$$\nu_{VRH} = \frac{1}{2}\left(1 - \frac{1}{\frac{1}{3} + \frac{K_{VRH}}{G_{VRH}}}\right) \tag{17}$$

10

where E_{VRH} and ν_{VRH} are the Young's modulus and Poisson's ratio of the equivalent isotropic matrix, respectively.

Single open microcrack-induced inelastic compliance tensor in the isotropic matrix

As in the previous works (Ju and Lee, 1991; Yu and Feng, 1995) under the tensile loading, only the opening microcracks are considered, and the effects of microcrack closure, frictional sliding and kinking are ignored.

Consider the α th single penny-shaped microcrack with radius a in the equivalent isotropic medium which is uniformly loaded at the far field. As exhibited in Fig. 2, the orientation of the microcrack can be expressed as (θ, ϕ) with the global coordinate system ($Ox_1x_2x_3$) and its corresponding local coordinate system ($Ox_1'x_2'x_3'$), where the x_2' axis is parallel to the normal vector of the microcrack $\mathbf{n}$, and the x_3' axis is coplanar with the x_1 axis and the x_3 axis.

The components of the displacement discontinuity vector of the α th microcrack take the form (Budiansky and O'Connell, 1976):

$$b_i = \left(a^2 - r^2\right)^{\frac{1}{2}} B'_{lj} \sigma'_{2j} g'_{li} \tag{18}$$

with

$$\sigma'_{2j} = g'_{2k} g'_{jl} \sigma_{kl} \tag{19}$$

$$g'_{ij} = g^T_{ij} = \begin{bmatrix} \cos\theta\cos\phi & \sin\theta & -\cos\theta\sin\phi \\ -\sin\theta\cos\phi & \cos\theta & \sin\theta\sin\phi \\ \sin\phi & 0 & \cos\phi \end{bmatrix} \tag{20}$$

where b_i are the components of the displacement discontinuity vector of the α th microcrack,

11

and $\mathbf{B}'$ is the crack opening displacement tensor which depends on the compliance of the microcrack-weakened solids. Assuming here that it depends only on the compliances of an isotropic elastic matrix, the nonvanishing components of $\mathbf{B}'$ for the open microcrack are (Yu and Feng, 1995)

$$B'_{11} = B'_{33} = \frac{16\left(1 - v_{VRH}^2\right)}{\left(2 - v_{VRH}^2\right)\pi E_{VRH}}, \quad B'_{22} = \frac{8\left(1 - v_{VRH}^2\right)}{\pi E_{VRH}} \quad (21)$$

The strains and compliances induced by the $\alpha\,th$ microcrack can be expressed by means of its opening displacements as:

$$\overline{\varepsilon}_{ij}^{*(\alpha)} = \overline{S}_{ijkl}^{*(a)}\,\overline{\sigma}_{kl} = \frac{1}{V}\int_{S_\alpha}\frac{1}{2}\left(b_i n_j + b_j n_i\right)^{(\alpha)} dS \quad (22)$$

where $\overline{\varepsilon}_{ij}^{*(\alpha)}$ and $\overline{S}_{ijkl}^{*(a)}$ are the strains and compliances induced by the $\alpha\,th$ microcrack; n_i represents those of the normal vector of the microcrack, and $\overline{\sigma}_{ij}$ denotes the volume-average stresses applied at the far field.

By substituting Eqs. (18)-(19) into Eq. (22), the compliances induced by the $\alpha\,th$ microcrack can be rephrased as follows (Yu and Feng, 1995):

$$\overline{S}_{ijkl}^{*(a)} = \frac{\pi a^3}{3V} B'_{mn} g'_{2k} g'_{nl}\left(g'_{mi} n_j + g'_{mj} n_i\right) \quad (23)$$

Overall microcrack-induced inelastic compliance tensor

To obtain the overall microcrack-induced inelastic compliance tensor, the integration procedures are employed over the RVE domain using the joint probability density function. The

orientations and sizes of penny-shaped microcracks in the RVE can be viewed as random variables and represented by a probability density function $p(a,\phi,\theta)$, which must satisfy the following normalization condition:

$$\int_{a_{\min}}^{a_{\max}} \int_0^{\frac{\pi}{2}} \int_0^{2\pi} p(a,\phi,\theta)\sin\phi\, d\phi\, d\theta\, da = 1 \tag{24}$$

In particular, when the penny-shaped microcracks are uniformly distributed in the orientation space with the same initial radius a_0, the overall inelastic effective compliance tensor caused by the stable microcracks can be expressed as:

$$\overline{\mathbf{S}}_{ijkl}^{*cs} = \sum_{k=1}^{N} \overline{\mathbf{S}}_{ijkl}^{*(a)} = \int_0^{\frac{\pi}{2}} \int_0^{2\pi} N_c\, p(\theta,\phi)\frac{\pi a^3}{3V} B'_{mn} g'_{2k} g'_{nl}\left(g'_{mi} n_j + g'_{mj} n_i\right)\sin\theta\, d\theta\, d\phi \tag{25}$$

with

$$p(\phi,\theta) = \frac{1}{2\pi} \tag{26}$$

where N_c is the total number of microcracks in the RVE.

The inelastic compliance tensor induced by the evolutionary microcracks

With the increase of the tensile loading, some microcracks in preferred orientations become unstable and increase in size. The damage-induced compliance can be divided into two parts. One is caused by the stable microcracks and the other is due to the evolutionary microcracks.

In reality, it is extremely difficult to give a unified criterion for pre-existing microcrack growth, if damage-induced anisotropic compliances and microcrack interaction are involved.

13

For simplification, linear elastic fracture mechanics is employed. The mixed-mode fracture criterion for a penny-shaped crack may take the following modified form (Ju and Lee, 1991):

$$\left(\frac{K_I'}{K_{IC}}\right)^2 + \left(\frac{K_{II}'}{K_{IIC}}\right)^2 = 1 \tag{27}$$

where K_I' and K_{II}' are the mode-I and mode-II stress intensity factors, respectively. K_{IC} and K_{IIC} are their critical values. Once the fracture criterion has been satisfied, a microcrack will become unstable, increasing its radius from the initial statistically averaged value a_0 to the final characteristic value a_u instantaneously, and will be arrested by energy barriers with higher strength (such as grain boundaries). It is noted that two assumptions of microcrack growth are made here. First, the microcrack growth process is assumed to be instantaneous (Krajcinovic and Fanella, 1986, Ju and Lee, 1991). Second, the penny-shaped microcrack growth is assumed to be in a self-similar fashion (Ju and Lee, 1991; Yu and Feng, 1995). For a specified uniaxial tension loading q, the mode-I and mode-II stress intensity factors can be expressed as follows (Ju and Lee, 1991; Yu and Feng, 1995)

$$K_I' = 2\sqrt{\frac{a}{\pi}}\bar{\tau}_3', \quad K_{II}' = \frac{4}{2-v}\sqrt{\frac{a}{\pi}}\bar{\tau}_4' \tag{28}$$

with

$$\bar{\tau}_3' = q\left(\cos\theta\right)^2, \quad \bar{\tau}_4' = q\cos\theta\sin\theta \tag{29}$$

By substituting Eqs. (28)-(29) into (27), we have

$$\left(\frac{2\sqrt{\dfrac{a}{\pi}}q(\cos\theta)^2}{K_{IC}}\right)^2 + \left(\frac{\dfrac{4}{2-\nu}\sqrt{\dfrac{a}{\pi}}q\cos\theta\sin\theta}{K_{IIC}}\right)^2 = 1 \tag{30}$$

After some lengthy but direct derivations, the critical angle θ_{cr} for the tensile loading q can be obtained as:

$$\left(\tan\theta_{cr}\right)^2 = \frac{-B-\sqrt{B^2-4AC}}{2A} \tag{31}$$

with

$$A = -\frac{\pi}{4a}K_{IIC}^2 \tag{32}$$

$$B = -\frac{\pi}{2a}K_{IIC}^2 + \left(\frac{2q}{2-\nu}\right)^2 \tag{33}$$

$$C = -\frac{\pi}{4a}K_{IIC}^2 + \left(\frac{qK_{IIC}}{K_{IC}}\right)^2 \tag{34}$$

With the critical angle θ_{cr}, the unstable domain can be obtained, which can be represented by $\Omega(\theta,\phi) = \{0 \le \theta \le \theta_r, 0 \le \phi \le 2\pi\}$. The compliance tensor due to the unstable microcracks can be calculated by the following integration:

$$\overline{\mathbf{S}}_{ijkl}^{*cu} = N\int_0^{\theta_{cr}}\int_0^{2\pi} p(\phi,\theta)\overline{\mathbf{S}}_{ijkl}^{*(a_u)}\sin\theta\, d\phi\, d\theta \tag{35}$$

Therefore, the compliance tensor induced by the stable and unstable microcracks can be represented as

15

$$\overline{\mathbf{S}}_{ijkl}^{*c} = \overline{\mathbf{S}}_{ijkl}^{*cs} + \overline{\mathbf{S}}_{ijkl}^{*cu}$$

$$= N \left[\int_{\theta_r}^{\frac{\pi}{2}} \int_0^{2\pi} p(\phi,\theta) \overline{\mathbf{S}}_{ijkl}^{*(a_0)} \sin\theta d\phi d\theta + \int_0^{\theta_r} \int_0^{2\pi} p(\phi,\theta) \overline{\mathbf{S}}_{ijkl}^{*(a_u)} \sin\theta d\phi d\theta \right] \quad (36)$$

16

Numerical simulations

Verifications with existing results

The proposed micromechanical damage framework aims to obtain the shale rock properties under tensile loading considering the material nanoscale microstructures. The total compliances are obtained by the sum of the undamaged and the microcrack-induced ones, which include those caused by the stable and evolutionary (unstable) microcracks. The verifications can be mainly classified into three categories. (i) For undamaged elastic compliance tensor of shale rock considering nanoscale microstructures, the estimations of our proposed model are compared with the available experimental data (Ortega et al., 2007). (ii) The existing predictions (Sayers and Kachanov, 1995) are utilized to prove the correctness of the stable microcrack-induced compliances obtained by our proposed model. (iii) To verify the compliance caused by the evolutionary microcracks, our predictions are compared with the existing experimental data (Gopalaratnam and Shah, 1985).

To attain the predicted undamaged elastic stiffness tensor, the model parameters of Ortega et al. (2007) are employed as the input, and consist of the material properties of the elementary phases present in shale rocks, including porosity, the five independent constants of the clay particle, the elastic properties and volume fraction of quartz inclusion. Table 1 shows the comparisons of the undamaged elastic stiffness tensor between our predictions and experimental data in Ortega et al. (2007). Our predictions match the experimental data well, with the average relative difference between them being 6.35%.

Sayers and Kachanov (1995) proposed an approximate scheme to estimate the

microcrack-induced compliance tensor for rock. In their work, the microcrack evolution was not considered. To further verify our proposed micromechanical damage model, the compliance tensors due to the stable microcracks are compared with those of Sayers and Kachanov (1995). According to their work, the additional compliance due to the microcracks can be expressed as:

$$\Delta S_{ijkl} = \frac{1}{4}\left(\delta_{ik}\alpha_{jl} + \delta_{il}\alpha_{jk} + \delta_{jk}\alpha_{il} + \delta_{jl}\alpha_{ik}\right) \tag{37}$$

with

$$\alpha_{ij} = \frac{1}{V}\sum_{r} B^r n_i^r n_j^r S_r \tag{38}$$

$$B^r = \frac{B_N + B_T}{2} \tag{39}$$

where n_i^r are the components of the normal vector of the *rth* microcrack, and δ_{ik} is the Kronecker delta. S_r is the area of the *rth* microcrack; B_N and B_T are the normal and shear terms of the crack compliance tensor, respectively.

The Young's modulus and Poisson's ratio of the isotropic matrix are 34 GPa and 0.3, respectively. From Figs. 3(a)-(b), it can be observed that our predictions for the different components of microcrack-induced compliance tensor are very close to those of Sayers and Kachanov (1995) with the increase of the microcrack density, which is $N_c a^3 / V$ in our presented model. Figs. 3(c)-(d) display the comparisons of the two results when different Poisson's ratios are considered, which also prove the effectiveness of our proposed model.

The concrete, similar to rock, is a microcrack-weakened brittle material (Ju and Lee, 1991), and the mechanical behaviours of these two materials can be characterized by similar constitutive equations (Ren et al., 2009; Ren et al., 2011; Xie et al., 2012). Fig. 4 shows the comparisons between the experimental data (Gopalaratnam and Shah, 1985) and the uniaxial

tensile stress-strain curve obtained by our proposed model. Both the stable and evolutionary microcrack induced compliances are considered in this example. It is observed that the analytical results are in a good agreement with the experimental results.

Influence of silt inclusions and porosity on the undamaged properties of shale rock matrix

In this section, the effects of silt inclusions and porosity are discussed on the properties of undamaged elastic shale rock matrix. The parameters of Ortega et al. (2007) are adopted as the input data for the transversely isotropic properties of clay particles. Similar to Ortega et al. (2007), only the quartz inclusions are considered, whose bulk modulus and shear modulus are 37.9 GPa and 44.3 GPa, respectively.

Fig. 5 presents the variations in the mechanical properties of the undamaged shale rock matrix with the increase of porosity. The volume fraction of the quartz inclusions is 20% here. Fig. 5(a) shows the evolution of different components of the stiffness tensor. It can be witnessed that the properties of the undamaged shale rock matrix (the pores-weakened solid matrix) gradually decrease when the porosity increases. Similar results can be found for the equivalent isotropic properties of the transversely isotropic pores-weakened solid matrix, which is displayed in Fig. 5(b).

Figs. 6(a)–(b) display the variations in the mechanical properties of the undamaged shale rock matrix with the increase of the volume fraction of the quartz inclusions. Since the properties of the quartz inclusions are much higher than those of micropore inclusions, the enhancing effects of quartz inclusions can be found on the material macroscopic properties. It can be witnessed that the values of the stiffness tensor become higher when the volume fraction

19

of quartz inclusions increases, as exhibited in Fig. 6(a). Similar variation tendencies can be observed for the equivalent isotropic properties of the transversely isotropic matrix, which is illustrated in Fig. 6(b).

Influence of silt inclusions and porosity on the microcrack-induced inelastic compliance tensor of shale rock

The material microstructures also play an important role in the damage evolution of shale rock. The parameters of Ortega et al. (2007) are again taken as the input data in our simulation work. Three different types of volume fractions of the quartz inclusions are employed as examples to illustrate the material microstructural effects on the stable microcrack-induced compliance. Figs. 7(a)-(b) present the variations in the stable microcrack-induced compliance tensor with increase of microcrack density. The three volume fractions of the quartz inclusions are 10%, 20% and 30%, respectively. It can be seen that the stable microcrack-induced compliance increases with the microcrack density, and the values increase when lower volume fractions of quartz inclusions are considered.

The microcrack-induced compliance tensors are also affected by the porosities. Here, three different porosities, which are 10%, 20% and 30%, respectively, are adopted as examples. From Figs. 8(a)–(b), it can be observed that with the increase of porosity, the microcrack-induced compliance becomes higher. Similarly, the higher the microcrack density is, the higher the microcrack-induced compliances become.

Fig. 9 and Fig. 10 exhibit the influence of quartz inclusions and porosity on the stress-strain relations of shale rock under tensile loading, respectively. From Fig. 9, it can be witnessed that

the strains, including the undamaged and the damage-induced strains, increase when lower volume fractions of the quartz inclusions are considered for the specified tensile loading. However, the total strains increase with higher porosities for a given tensile loading, as exhibited in Fig. 10.

Conclusions

Inspired by current micromechanical damage models for shale rocks (Sayers and Kachanov, 1995; Sayers, 2005; Ougier-Simonin et al., 2009), our extension proposes a simplified multiscale damage framework for transversely isotropic shale rock under tensile loading. Firstly, the multiscale representations for shale rock are presented by introducing the microcrack-weakened equivalent solid with hierarchical microstructures. Secondly, the shale rocks' transversely isotropic undamaged properties are obtained by performing multilevel homogenizations. The equivalent isotropic medium is attained using the Voigt–Reuss–Hill averages of the material transversely isotropic properties. Meanwhile, the microcrack-induced compliance tensors, including those caused by the stable and unstable microcracks, are reached with the microcrack opening displacements in the equivalent isotropic medium. Finally, numerical examples including experimental validations and comparisons with existing micromechanical models are presented. From this study, the following main conclusions can be drawn:

(1) Comparisons with the available experimental data show that our proposed multiscale damage framework is feasible and capable of predicting mechanical performance of shale rocks under tensile loading.

(2) The silt components in shale rocks, such as quartz inclusions, can improve the

components of the material stiffness tensor, which will reduce the material strain or compliance, including the undamaged elastic one and the microcrack-induced one, for a specified tensile loading.

(3) The (micro-)pores cause deterioration of the solid phase of the shale rock, which will increase the material strain or compliance given a specified tensile loading. The damage-induced strain or compliance of shale rock will increase when the microcrack density is higher.

References

Bayuk IO, Ammerman M and Chesnokov EM (2008) Upscaling of elastic properties of anisotropic sedimentary rocks. *Geophysical Journal International* 172(2): 842–860.

Berryman JG (1980) Long-wave propagation in composite elastic media II. Ellipsoidal inclusion. *Journal of the Acoustical Society of America* 68(6): 1820–1831.

Bobko CP, Gathier B, Ortega JA, Ulm FJ, Borges L, and Abousleiman YN (2011) The nanogranular origin of friction and cohesion in shale-A strength homogenization approach to interpretation of nanoindentation results. *International Journal for Numerical and Analytical Methods in Geomechanics* 35: 1854–1876.

Bobko CP and Ulm FJ (2008) The nano-mechanical morphology of shale. *Mechanics of Materials* 40: 318–337.

Budiansky B and O'connell RJ (1976) Elastic moduli of a cracked solid. *International Journal of Solids and Structures* 12: 81–97.

Chang C, Zoback MD and Khaksar A (2006) Empirical relations between rock strength and physical properties in sedimentary rocks. *Journal of Petroleum Science and Engineering* 51:223–237.

Chen Q, Zhu HH, Ju JW, Guo F, Wang LB, Yan ZG, Deng T and Zhou S (2015a) A stochastic micromechanical model for multiphase composite containing spherical inhomogeneities. *Acta Mechanica* 226(6): 1861–1880.

Chen Q, Zhu HH, Yan ZG, Deng and Zhou S (2015b) Micro-scale description of the saturated concrete repaired by electrochemical deposition method based on Mori-Tanaka method. *Journal of Building Structures* 36(1): 98–103.

Chen Q, Zhu HH, Yan ZG, Ju JW, Deng T and Zhou S (2015c) Micro-scale description of the saturated concrete repaired by electrochemical deposition method based on self-consistent method. *Chinese Journal of Theoretical and Applied Mechanics* 47(2): 367–371.

Chen YY, Furmann A, Mastalerz M and Schimmelmann A (2014a) Quantitative analysis of shales by KBr-FTIR and micro-FTIR. *Fuel* 116: 538–549.

Chen YY, Mastalerz M and Schimmelmann A (2014b). Heterogeneity of shale documented by micro-FTIR and image analysis. *Journal of Microscopy* 256(3): 177-189.

Chudnovsky A, Dolgopolsky A and Kachanov M (1987a) Elastic interaction of a crack with a microcrack array-I: formulation of the problem and general form of the solution. *International Journal of Solids and Structures* 23: 1–10.

Chudnovsky A, Dolgopolsky A and Kachanov M (1987b) Elastic interaction of a crack with a microcrack array-II: elastic solution for two crack configurations. *International Journal of Solids and Structures* 23:11–21.

Dewhurst DN, Sarout J, Piane CD, Siggins AF and Raven MD (2015) Empirical strength prediction for preserved shales. *Journal of Petroleum Geology* 67: 512–525.

Fanella D and Krajcinovic D (1988) A micromechanical model for concrete in compression. *Engineering Fracture Mechanics* 29: 49–66.

Farrokhrouz M, Asef RM and Kharrat R (2014) Empirical estimation of uniaxial compressive strength of shale formations. *Geophysics* 79:D227-D233.

Giraud A, Huynh QV, Hoxha D and Kondo D (2007) Application of results on Eshelby tensor to the determination of effective poroelastic properties of anisotropic rocks-like composites.

23

International Journal of Solids and Structures 44: 3756–3772.

Gopalaratnam VS and Shah SP (1985) Softening response of plain concrete in direct tension. *ACI Materials Journal* May/June: 310–323.

Guo ZQ, Li XY, Liu C, Feng X and Shen Y (2013) A shale rock physics model for analysis of brittleness index, mineralogy and porosity in the Barnett Shale. *Journal of Geophysics and Engineering* 10: 1–10.

Hoenig A (1979) Elastic moduli of a non-randomly cracked body. *International Journal of Solids and Structures* 15: 137–154.

Horii H and Nemat-Nasser S (1983) Overall moduli of solids with microcracks: load-induced anisotropy. *Journal of the Mechanics and Physics of Solids* 31: 155–171.

Horii H and Nemat-Nasser S (1985) Elastic fields of interacting inhomogeneities. *International Journal of Solids and Structures* 21: 731–745.

Hornby BE, Schwartz LM and Hudson JA (1994) Anisotropic effective-medium modeling of the elastic properties of shales. *Geophysics* 59(10): 1570–1583.

Johnston JE and Christensen NI (1995) Seismic anisotropy of shales. *Journal of Geophysical Research* 100(B4): 5991–6003.

Josh M, Esteban L, Delle Piane C, Sarout J, Dewhurst DN and Clennell MB (2012) Laboratory characterisation of shale properties. *Journal of Petroleum Science and Engineering* 88-89: 107–124.

Ju JW (1989) On energy-based coupled elastoplastic damage theories: constitutive modeling and computational aspects. *International Journal of Solids and Structures* 25: 803–833.

Ju JW (1991) On two-dimensional self-consistent micromechanical damage models for brittle solids. *International Journal of Solids and Structures* 27: 227–258.

Ju JW and Lee X (1991) Micromechanical damage models for brittle solids. Part I: tensile loadings. *Journal of Engineering Mechanics* 117: 1495–1514.

Ju JW, Monteiro PJM and Rashed AI (1989) On continuum damage of cement paste and mortar as affected by porosity and sand concentration. *Journal of Engineering Mechanics* 115: 105–130.

Ju JW and Chen TM (1994a) Effective elastic moduli of two-phase composites containing randomly dispersed spherical inhomogeneities. *Acta Mechanica* 103: 123–144.

Ju JW and Chen TM (1994b) Micromechanics and effective moduli of elastic composites containing randomly dispersed ellipsoidal inhomogeneities. *Acta Mechanica* 103: 103–121.

Ju JW and Sun LZ (1999) A novel formulation for the exterior-point Eshelby's tensor of an ellipsoidal inclusion. *Journal of Applied Mechanics-Transactions of the ASME* 66(2): 570–574.

Ju JW and Sun LZ (2001) Effective elastoplastic behavior of metal matrix composites containing randomly located aligned spheroidal inhomogeneities. Part I: micromechanics-based formulation. *International Journal of Solids and Structures* 38(2): 183–201.

Ju JW and Yanase K (2010) Micromechanics and effective elastic moduli of particle-reinforced composites with near-field particle interactions. *Acta Mechanica* 215 (1): 135–153.

Ju JW and Yanase K (2011) Micromechanical effective elastic moduli of continuous fiber-reinforced composites with near-field fiber interactions. *Acta Mechanica* 216 (1): 87–103.

Ju JW and Zhang XD (1998) Micromechanics and effective transverse elastic moduli of composites with randomly located aligned circular fibers. *International Journal of Solids and Structures* 35(9-10): 941–960.

Kachanov M (1987) Elastic solids with many cracks: a simple method of analysis. *International Journal of Solids and Structures* 23: 23–43.

Krajcinovic D (1984) Continuous damage mechanics. *Applied Mechanics Reviews* 37: 1–6.

Krajcinovic D and Sumarac D (1989) A mesomechanical model for brittle deformation processes. I. *Journal of Applied Mechanics* 56: 51–56.

Krajcinovic D and Fanella D. (1986) A micromechanical model for concrete, *Engineering Fracture Mechanics* 25: 585–596.

Levin VM and Markov MG (2005) Elastic properties of inhomogeneous transversely isotropic rocks. *International Journal of Solids and Structures* 42 (2): 393–408.

Li GQ, Zhao Y and Pang SS (1999) Four-phase sphere modeling of effective bulk modulus of concrete. *Cement and Concrete Research*. 29: 839–845.

Norris A (1985) A differential scheme for the effective moduli of composites. *Mechanics of Materials* 4(1), 1–16.

Ortega JA, Ulm FJ and Abousleiman Y (2007) The effect of the nanogranular nature of shale on their poroelastic properties. *Acta Geotechnica* 2(3), 155–182.

Ougier-Simonin A, Sarout J and Guéguen Y (2009) A simplified model of effective elasticity for anisotropic shales. *Geophysics* 74(3), D57–D63.

Ren ZJ, Peng XH, Hu N and Yang CH (2009) A micromechanical damage model for rocks and concretes under triaxial compression. *Applied Mathematics and Mechanics*. 30(3), 323–333.

Ren ZJ, Peng XH and Wan L (2011) A three-dimensional micromechanics model for the damage of brittle materials based on the growth and unilateral effect of elliptic microcracks, *Engineering Fracture Mechanics* 78: 274–288.

Sarout J and Guéguen Y (2008a) Elastic wave velocities evolution in experimentally deformed anisotropic shales — Part 1: Experimental results. *Geophysics* 73(5): D75–D89.

Sarout J and Guéguen Y (2008b) Elastic wave velocities evolution in experimentally deformed anisotropic shales — Part 2: Modeling results. *Geophysics* 73(5): D91–D103.

Sayers C (2005) Seismic anisotropy of shales. *Geophysical Prospecting* 53:667–676.

Sayers C and Kachanov M (1995) Microcracks-induced elastic wave anisotropy of brittle rocks: *Journal of Geophysical Research* 100: 4149–4156.

Sayers CM (1994) The elastic anisotropy of shales. *Journal of Geophysical Research* 99(B1): 767–774.

Sayers CM (1999) Stress-dependent seismic anisotropy of shales. *Geophysics* 64(1): 93–98.

Sayers CM (2005) Seismic anisotropy of shales. *Geophysical Prospecting* 53(5): 667–676.

Simo JC and Ju JW (1987a) Strain- and stress-based continuum damage models—I. Formulation. *International Journal of Solids and Structures* 23: 821–840.

Simo JC and Ju JW (1987b) Strain-and stress-based continuum damage models—II. Computational aspects. *International Journal of Solids and Structures* 23: 841–869.

Simo JC and Ju JW (1989) On continuum damage-elastoplasticity at finite strains: a computational framework. *Computational Mechanics* 5: 375–400.

Sumarac D and Krajcinovic D (1987) A self-consistent model for microcrack-weakened solids. *Mechanics of Materials* 6: 39–52.

Thomsen L (2001) Seismic anisotropy. *Geophysics* 66(1): 40–41.

Ulm FJ and Abousleiman Y (2006) The nanogranular nature of shale. *Acta Ceotechnica* 1(2):77–88.

Xie N, Zhu QZ, Shao JF and Xu LH (2012) Micromechanical analysis of damage in saturated quasi brittle materials. *International Journal of Solids and Structures* 49: 919–928.

Yan ZG, Chen Q, Zhu HH, Ju JW, Zhou S and Jiang ZW (2013) A multiphase micromechanical model for unsaturated concrete repaired by electrochemical deposition method. *International Journal of Solids and Structures* 50(24): 3875–3885.

Yu SW and Feng XQ (1995) A micromechanics-based damage model for microcrack-weakened brittle solids. *Mechanics of Materials* 20: 59–76.

Zhu HH, Chen Q, Ju JW, Yan ZG, Guo F, Wang YQ, Jiang ZW, Zhou S and Wu B (2015) Maximum entropy based stochastic micromechanical model for two-phase composite considering the inter-particle interaction effect. *Acta Mechanica* 226(9): 3069–3084.

Zhu HH, Chen Q, Yan ZG, Ju JW and Zhou S (2014) Micromechanical model for saturated concrete repaired by electrochemical deposition method. *Materials and structures* 47: 1067–1082.
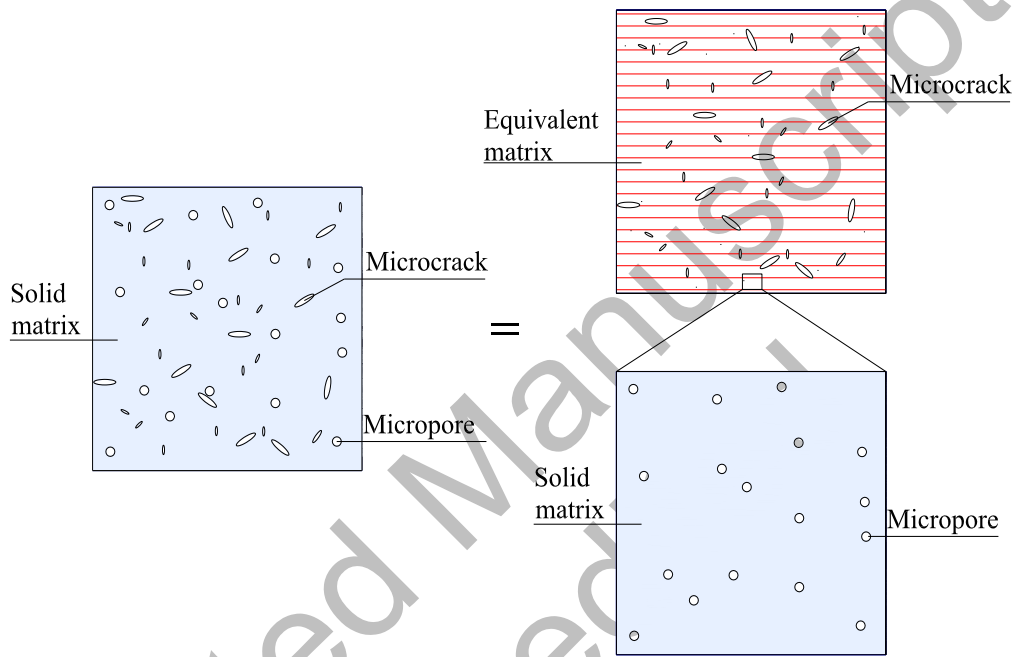
(a) The RVE decomposition for the microcracked shale rock
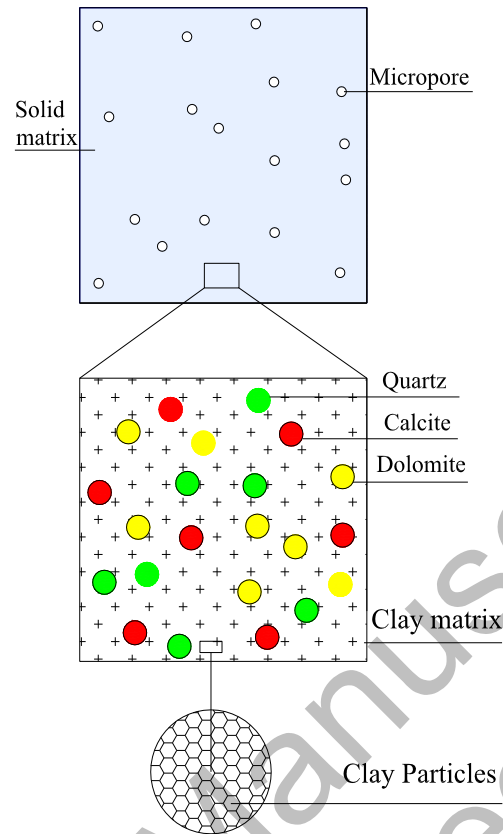
(b) The multiscale representation for the porous matrix

Fig. 1   The multiscale representation for the microcrack weakened shale rock
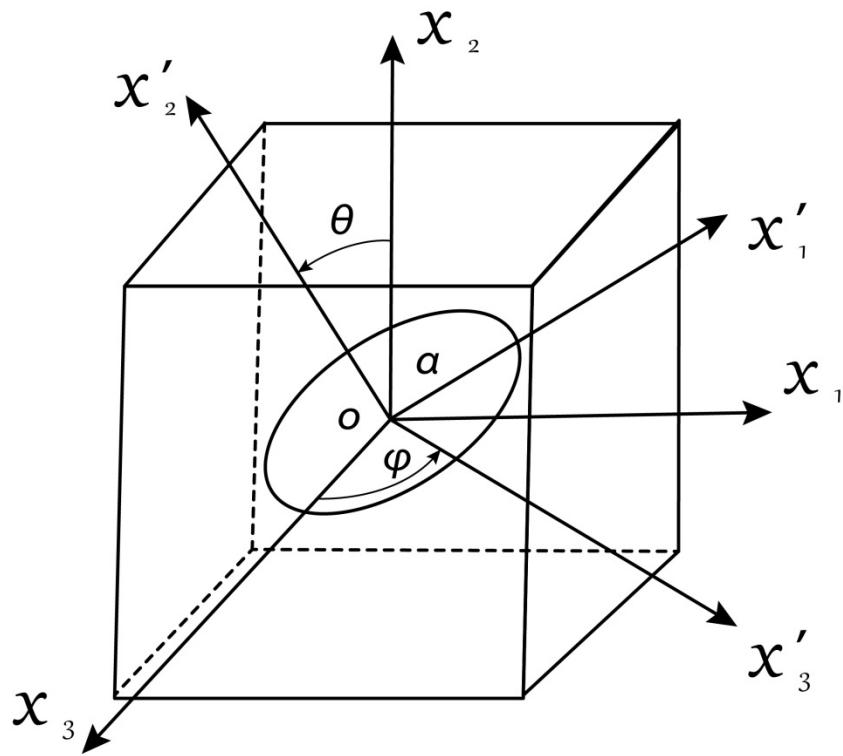
Fig. 2   The local coordinate system for a microcrack
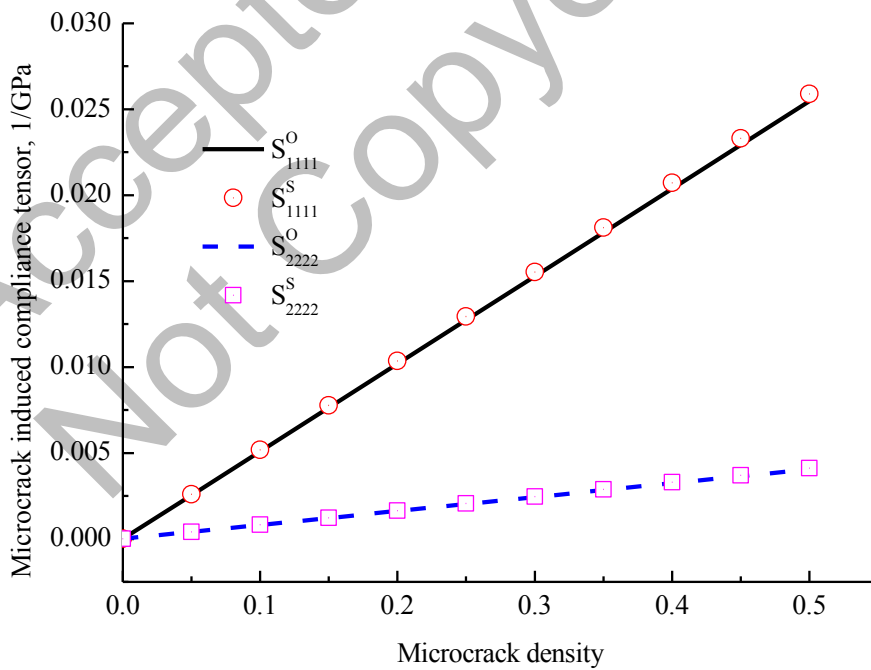
(a)
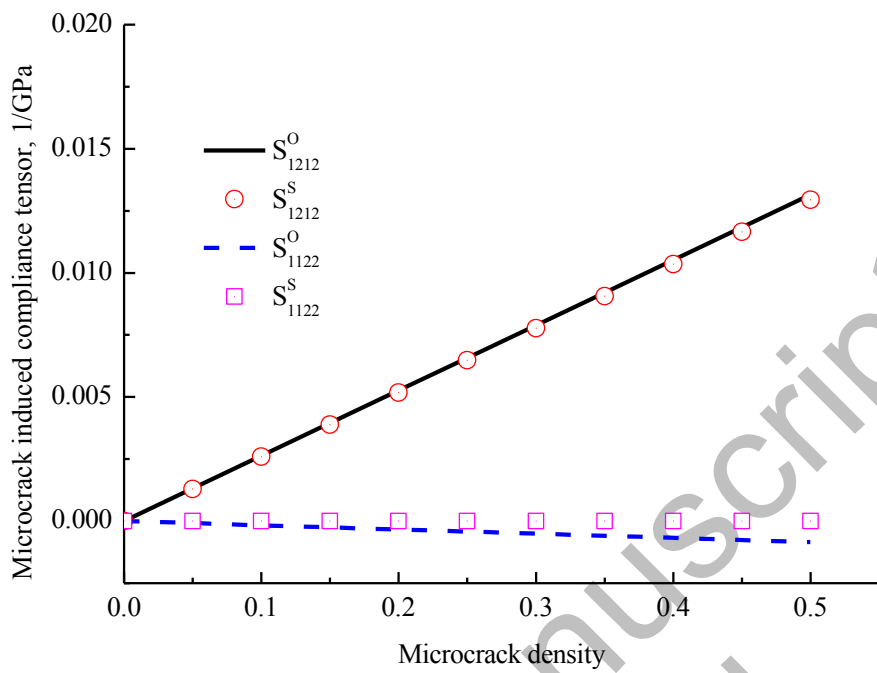
(b)
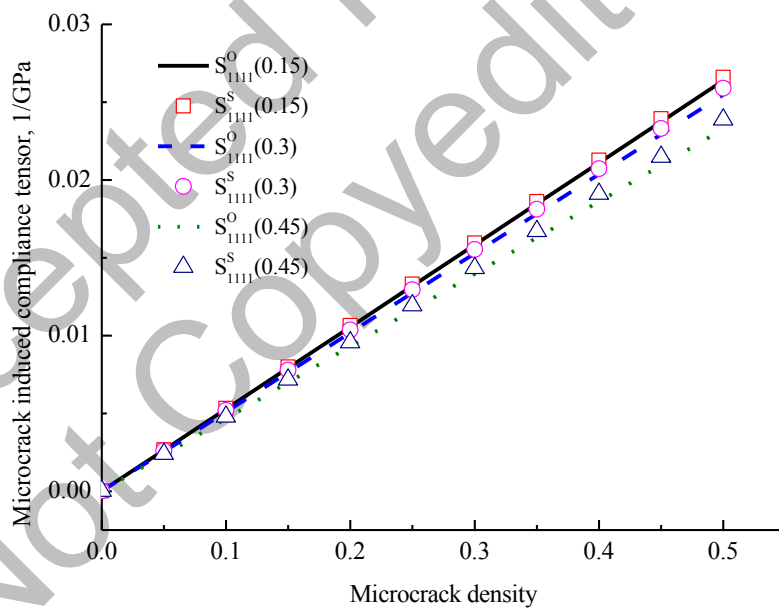
(c)
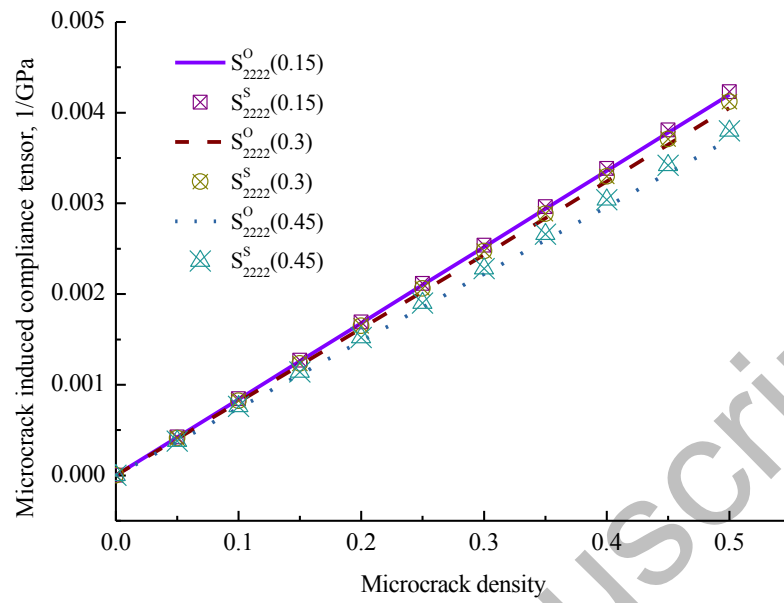
(d)

Fig.3 Comparisons between our results and those of Sayers and Kachanov (1995), with superscript O and S representing results obtained by our model and Sayers and Kachanov's model (Sayers and Kachanov,1995), with the data in the brackets representing the Poisson's ratio
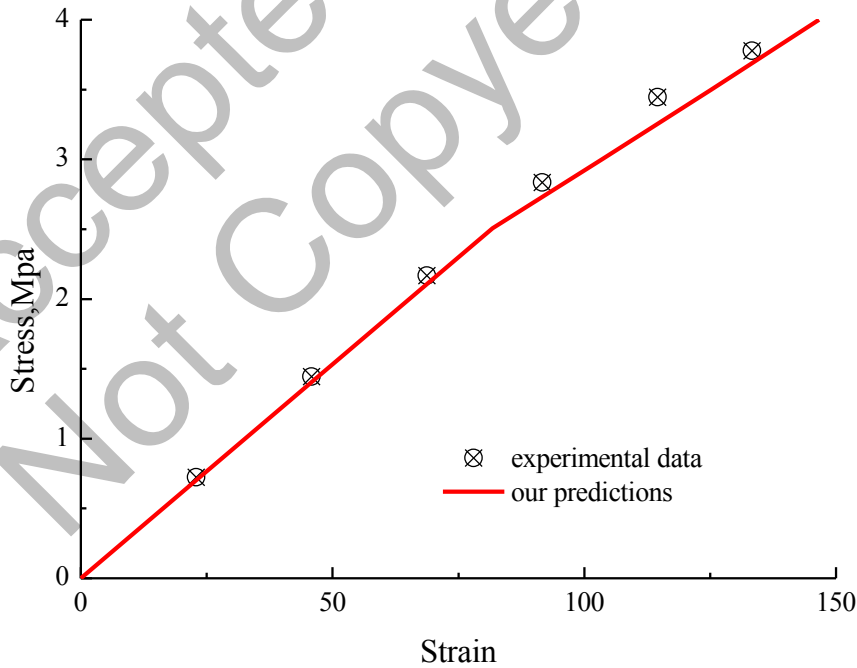
Fig. 4 The comparisons between the experimental data (Gopalaratnam and Shah, 1985) and the uniaxial tensile stress-strain curve obtained by our proposed model.
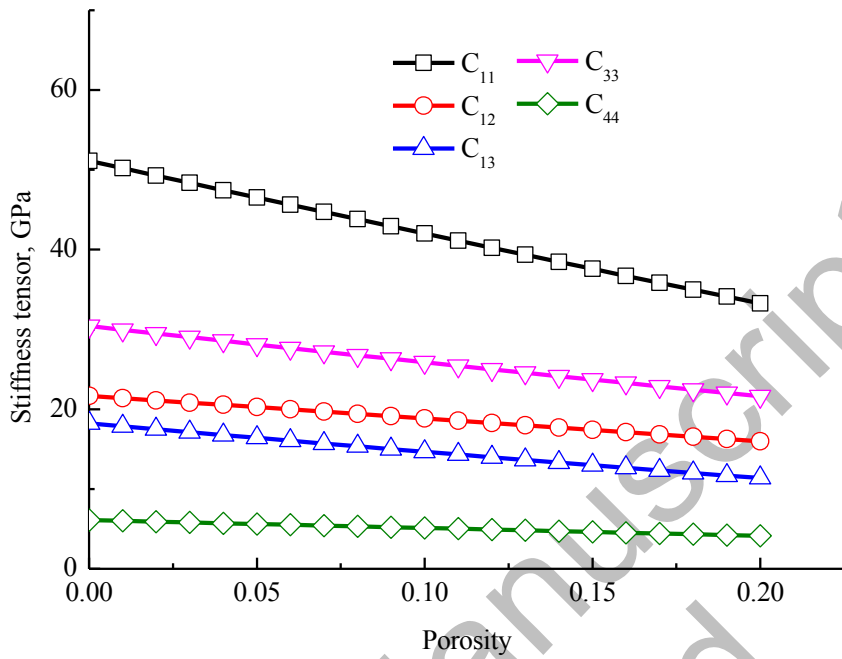
(a) Influence of porosity on the properties of undamaged shale rock matrix
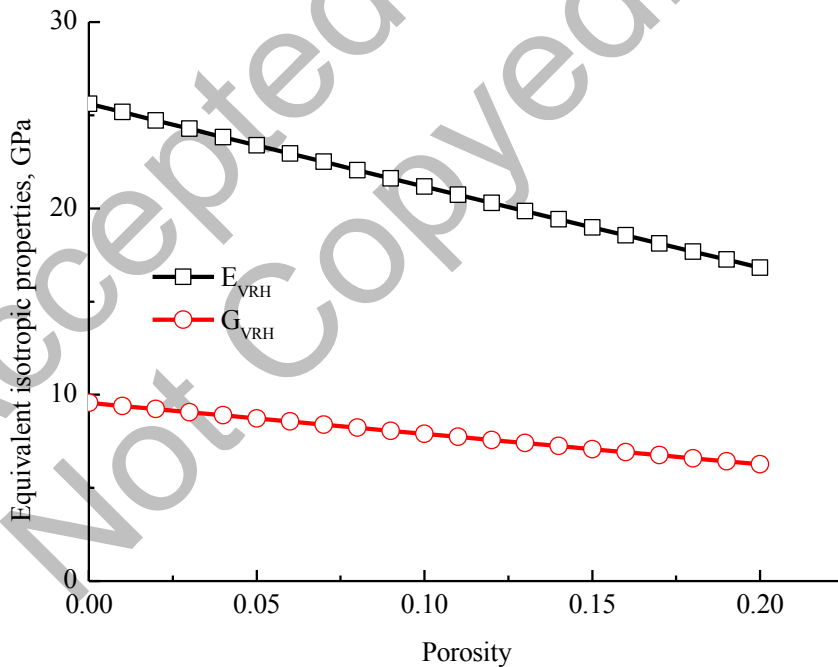
(b) Influence of porosity on the equivalent isotropic properties

Fig. 5 The variations in the mechanical properties of the undamaged elastic shale rock matrix with the increase of porosity.
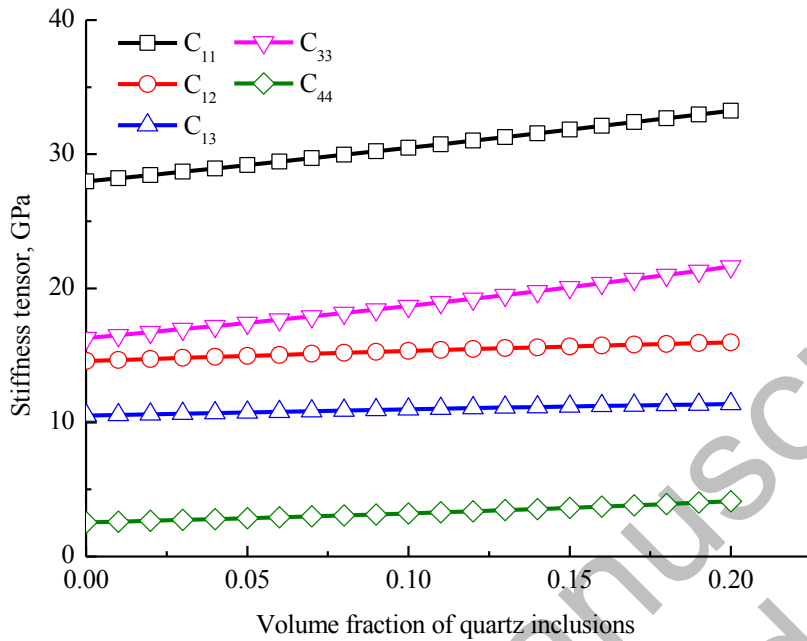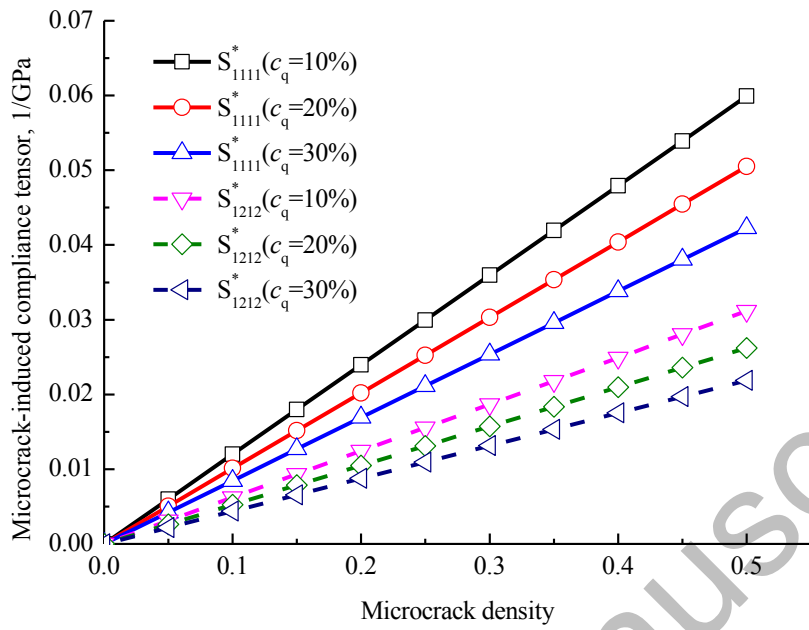
(a) Influence of quartz inclusions on the properties of undamaged shale rock matrix
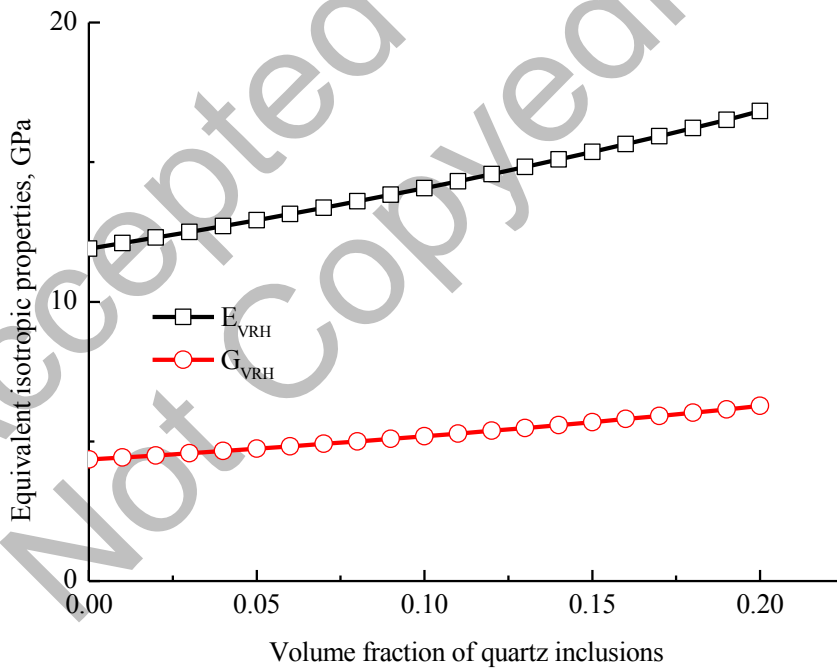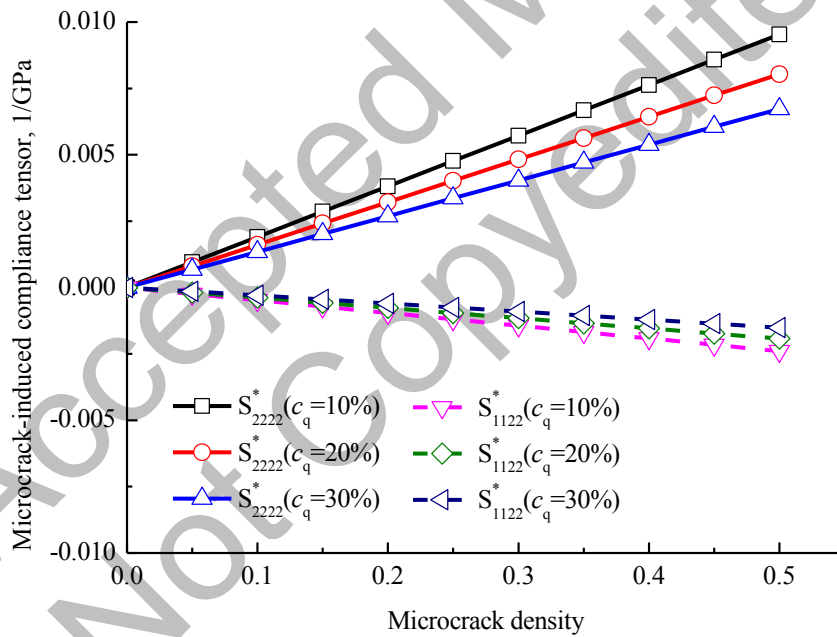

(b) Influence of quartz inclusions on the equivalent isotropic properties

Fig. 6 The variations in the mechanical properties of the undamaged elastic shale rock

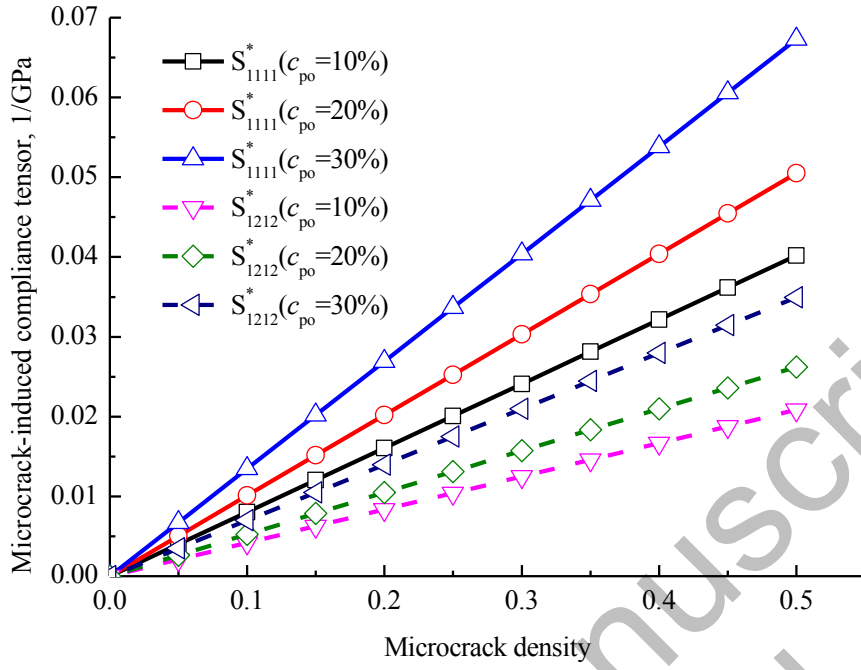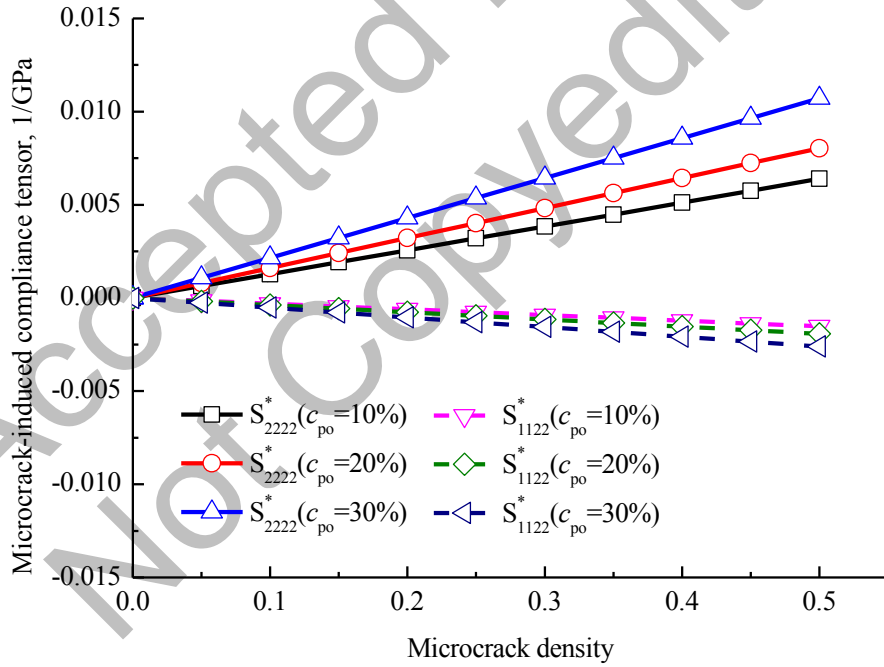matrix with the increase of quartz inclusions

(a)

(b)

Fig. 7 Influence of quartz inclusions on the stable-microcrack induced compliance tensor

(a)

(b)

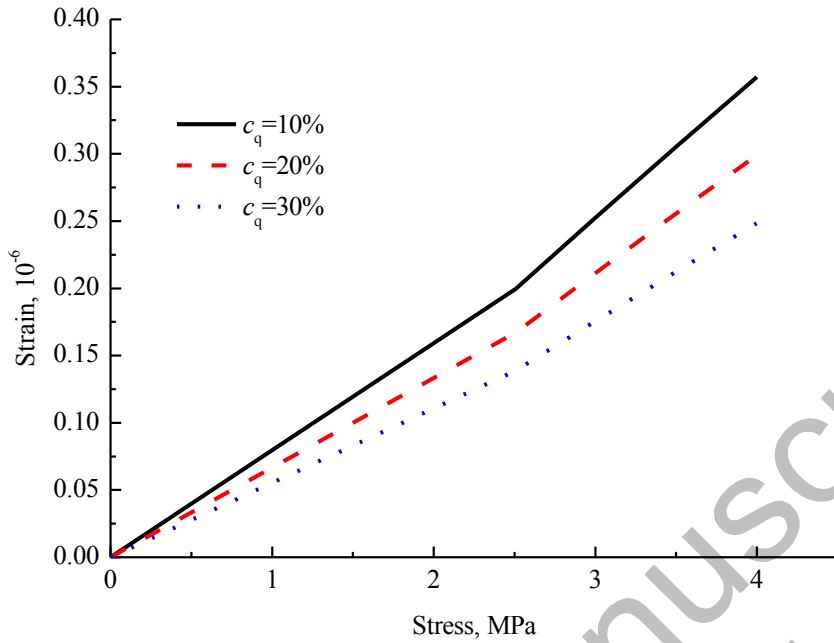**Fig. 8** Influence of porosity on the stable-microcrack induced compliance tensor

Fig. 9　Influence of quartz inclusions on the stress-strain relation of shale rock under tensile loading (including the stable and evolutionary microcrack induced compliance)
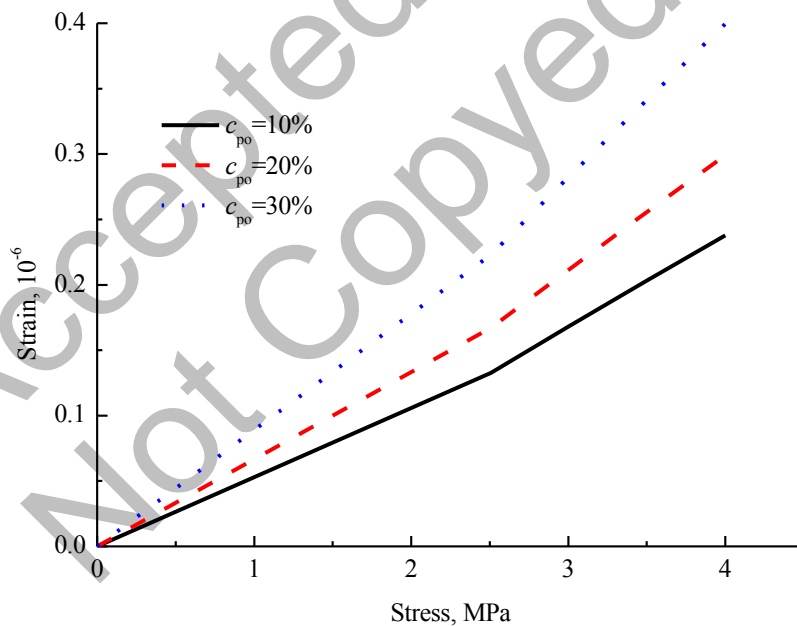

Fig. 10　Influence of porosity on the stress-strain relation of shale rock under tensile loading (including the stable and evolutionary microcrack induced compliance)

Table 1 Comparison of undamaged elastic stiffness tensor between our predictions and experimental data in Ortega et al. (2007), with C_e, C_o and RD representing the experimental data, our predictions and the relative difference between them (Elastic constants in GPa).

	G03			G06			G07		
	C_e	C_o	RD	C_e	C_o	RD	C_e	C_o	RD
C_{11}	46.1	47.7	3.4%	38.9	38.7	-0.5%	45.8	48.2	5%
C_{12}	17.8	19.6	10.1%	13.8	18.1	31.1%	17.7	19.7	11.2%
C_{33}	30.4	30.8	1.4%	20.4	23.4	14.7%	29.7	31.2	5.1%
C_{44}	5.8	6.9	19.0%	4.5	4.4	-3%	8.9	7.0	-21.0%